Chapter 9

Eilenberger Approach to the Vortex State in Iron Pnictide Superconductors

I. Zakharchuk, P. Belova, K. B. Traito and E. Lähderanta

Additional information is available at the end of the chapter

http://dx.doi.org/10.5772/48571

1. Introduction

The SC gap, which characterizes the energy cost for breaking a Cooper pair, is an important quantity when clarifying the SC mechanism. The gap size and its momentum dependence reflect the strength and anisotropy of the pairing interactions, respectively. Some experiment executed by Li *et al*. [1] in response to a suggestion by Klemm [2] tested the phase of the wave function in $Bi_2Sr_2CaCu_2O_8$ and revived the *s*-wave viewpoint [3, 4]], which, although championed by Dynes's group [4], had been out of favor even for $Bi_2Sr_2CaCu_2O_8$, although not disproven. This experiment once more created uncertainty over whether the superconducting pairs are consistent with *s*-wave or *d*-wave superconductivity (Van Harlingen [5], Ginsberg [6], Tsuei and Kirtley [7]).

The discovery of Fe-based superconductors [8] generated intensive debate on the superconducting (SC) mechanism. Motivated by high-T_c values up to 56 K [9], the possibility of unconventional superconductivity has been intensively discussed. A plausible candidate is the SC pairing mediated by antiferromagnetic (AFM) interactions. Two different approaches, based on the itinerant spin fluctuations promoted by Fermi-surface (FS) nesting [10, 11], and the local AFM exchange couplings [12], predict the so-called $s^{\pm}$-wave pairing state, in which the gap shows a *s*-wave symmetry that changes sign between different FSs. Owing to the multiorbital nature and the characteristic crystal symmetry of Fe-based superconductors, s_{++}-wave pairing without sign reversal originating from novel orbital fluctuations has also been proposed [13, 14]. The unconventional nature of the superconductivity is supported by experimental observations such as strongly FS-dependent anomalously large SC gaps [15–17] and the possible sign change in the gap function [18, 19] on moderately doped $BaFe_2As_2$, NdFeAsO and $FeTe_{1-x}Se_x$. However, a resonance like peak structure, observed by neutron scattering measurements [18], is reproduced by considering the strong correlation effect via quasiparticle damping, without the necessity of sign reversal in the SC gap [20]. Although the $s^{\pm}$-wave state is expected to be very fragile as regards impurities due to the interband scattering [21], the superconducting state is remarkably robust regarding impurities and α-particle irradiation [22].

There is growing evidence that the superconducting gap structure is not universal in the iron-based superconductors [23, 24]. In certain materials, such as optimally doped $BaKFe_2As_2$ and $BaFeCo_2As_2$, strong evidence for a fully gapped superconducting state has been observed from several low-energy quasiparticle excitation probes, including magnetic penetration depth [25, 26], and thermal conductivity measurements [27]. In contrast, significant excitations at low temperatures due to nodes in the energy gap have been detected in several Fe-pnictide superconductors. These include LaFePO ($T_c = 6$ K) [28, 29], $BaFe_2AsP_2$ ($T_c = 31$ K) [30–32], and KFe_2As_2 ($T_c = 4$ K) [33, 34].

At a very early stage, it was realized that electron and hole doping can have qualitatively different effects in the pnictides [35]. Hole doping should increase the propensity to a nodeless ($s^{\pm}$) SC phase. The qualitative picture applies to both the "122" as the "1111" compounds: As the Fermi level is lowered, the M h pocket becomes more relevant and the $M \leftrightarrow X$ scattering adds to the $(\pi, 0)/(0, \pi)$ scattering from Γ to X. As such, the anisotropy-driving scattering, such as interelectron pocket scattering, becomes less relevant and yields a nodeless, less anisotropic, and more stable $s^{\pm}$ [36]. This picture is qualitatively confirmed by experiments. While thermoelectric, transport, and specific heat measurements have been performed for $K_xBa_{1-x}Fe_2As_2$ from $x = 0$ to the strongly hole-doped case $x = 1$ [37, 38], more detailed studies have previously focused on the optimally doped case $x = 0.4$ with $T_c = 37$ K, where all measurements such as penetration depth and thermal conductivity find indication for a moderately anisotropic nodeless gap [39, 40]. Similarly, angle-resolved photoemission spectroscopy (ARPES) on doped $BaFe_2As_2$ reveals a nodeless SC gap [16, 41].

The experimental findings for the SC phase in KFe_2As_2 were surprising. Thermal conductivity [33], penetration depth [34], and NMR [42] provide a clear indication of nodal SC. The critical temperature for KFe_2As_2 is $\sim$ 3 K, an order of magnitude less than the optimally doped samples. ARPES measurements [43] show that the e pockets have nearly disappeared, while the h pockets at the folded Γ point are large and have a linear dimension close to π/a. A detailed picture of how the SC phase evolves under hole doping in $K_xBa_{1-x}Fe_2As_2$ was found and that the nodal phase observed for $x = 1$ is of the (extended) d-wave type [44]. The functional renormalization group was used to investigate how the SC form factor evolves under doping from the nodeless anisotropic $s^{\pm}$ in the moderately hole-doped regime to a d-wave in the strongly hole-doped regime, where the e pockets are assumed to be gapped out. The d-wave SC minimizes the on-pocket hole interaction energy. It was found that the critical divergence scale to be of an order of magnitude lower than for the optimally doped $s^{\pm}$ scenario, which is consistent with experimental evidence [44].

The synthesis of another iron superconductor immediately attracted much attention for several reasons [9, 45]. LiFeAs is one of the few superconductors which does not require additional charge carriers and is characterized by T_c approaching the boiling point of hydrogen. Similar to $AeFe_2As_2$ (Ae = Ba, Sr, Ca "122") and LnOFeAs ("1111") parent compounds, LiFeAs ($T_c = 18$ K) consists of nearly identical $(Fe_2As_2)^{2-}$ structural units and all three are isoelectronic, though the former do not superconduct. The band structure calculations unanimously yield the same shapes for the FS, as well as very similar densities of states, and low energy electronic dispersions [46, 47]. Moreover the calculations even find in LiFeAs an energetically favorable magnetic solution which exactly corresponds to the famous stripelike antiferromagnetic order in "122" and "1111" systems [46, 48]. The experiments, however, show a rather different situation. The structural transition peculiar to "122" and "1111" families is remarkably absent in LiFeAs and is not observed under an applied pressure

of up to 20 GPa [49]. Resistivity and susceptibility as well as μ-spin rotation experiments show no evidence of magnetic transition [50, 51]. Only a weak magnetic background [51] and field induced magnetism in the doped compound have been detected [50]. What was identified was a notable absence of the Fermi surface nesting, a strong renormalization of the conduction bands by a factor of 3, a high density of states at the Fermi level caused by a van Hove singularity, and no evidence of either a static or a fluctuating order; although superconductivity with in-plane isotropic energy gaps have been found implying the s_{++} pairing state [52]. However, a gap anisotropy along the Fermi surface up to $\sim$ 30% was observed in Ref. [53]. Thus, the type of the superconducting gap symmetry in LiFeAs is still an open question.

The aim of our paper is to apply quasiclassical Eilenberger approach to the vortex state considering $s^{\pm}$, s_{++} and $d_{x^2-y^2}$-wave pairing symmetries as presumable states for the different levels of impurity scattering rates Γ^*, to calculate the cutoff parameter ξ_h [54, 55] and to compare results with experimental data for iron pnictides. As described in Ref. [56], ξ_h is important for the description of the muon spin rotation (μSR) experiments and can be directly measured.

The London model used for the analysis of the experimental data does not account for the spatial dependence of the superconducting order parameter and it fails down at distances of the order of coherence length from the vortex core center, *i.e.*, $B(r)$ logarithmically diverges as $r \to 0$. To correct this, the **G** sum in the expression for the vortex lattice free energy can be truncated by multiplying each term by a cutoff function $F(G)$. Here, **G** is a reciprocal vortex lattice vector. In this method the sum is cut off at high $G_{max} \approx 2\pi/\xi_h$, where ξ_h is the cutoff parameter. The characteristic length ξ_h accommodates a number of inherent uncertainties of the London approach; the question was discussed originally by de Gennes group [57] and discussed in some detail in Ref. [58]. It is important to stress that the appropriate form of $F(G)$ depends on the precise spatial dependence of the order parameter in the the vortex core region, and this, in general, depends on the temperature and the magnetic field.

A smooth Gaussian cutoff factor $F(G) = exp(-\alpha G^2\xi^2)$ was phenomenologically suggested. Here, ξ is the Gizburg-Landau coherence length. If there is no dependence of the superconducting coherence length on temperature and magnetic field, then changes in the spatial dependence of the order parameter around a vortex correspond to changes in α. By solving the Ginzburg-Landau (GL) equations, Brandt determined that $\alpha = 1/2$ at fields near B_{c2} [59], and arbitarily determined it to be $\alpha \approx 2$ at fields immediately above B_{c1} [60]. For an isolated vortex in an isotropic extreme (the GL parameter $\kappa_{GL} \gg 1$) *s*-wave superconductor, α was obtained by numerical calculation of GL equations. It was found that α decreases smoothly from $\alpha = 1$ at B_{c1} to $\alpha \approx 0.2$ at B_{c2} [61]. The analytical GL expression was obtained by [62] for isotropic superconductors at low inductions $B \ll B_{c2}$. Using a Lorentzian trial function for the order parameter of an isolated vortex, Clem found for large $\kappa_{GL} \gg 1$ that $F(G)$ is proportional to the modified Bessel function. In Ref. [63], the Clem model [62] was extended to larger magnetic fields up to B_{c2} through the linear superposition of the field profiles of individual vortices. In this model, the Clem trial function [62] is multiplied by a second variational parameter f_∞ to account for the suppression of the order parameter due to the overlapping of vortex cores. This model gave the method for calculating the magnetization of type-II superconductors in the full range $B_{c1} < B < B_{c2}$. Their analytical formula is in a good agreement with the well-known Abrikosov high-field result and considerably corrects the results obtained with an exponential cutoff function at

low fields [64]. This approximation was widely used for the analysis of the experimental data on magnetization of type-II superconductors (see references 27-29 in Ref. [65]). The improved approximate Ginzburg-Landau solution for the regular flux-line lattice using circular cell method was obtained in Ref. [65]. This solution gives better correlation with the numerical solution of GL equations.

The Ginzburg-Landau theory, strictly speaking, is only valid near T_c but it is often used in the whole temperature range taking the cutoff parameter ξ_h and penetration depth λ as a fitting parameters. Recently, an effective London model with the effective cutoff parameter $\xi_h(B)$ as a fitting parameter was obtained for clean [54] and dirty [55] superconductors, using self-consistent solution of quasiclassical nonlinear Eilenberger equations. In this approach, λ is not a fitting parameter but calculated from the microscopical theory of the Meissner state. As was shown in Ref. [66], the reduction of the amount of the fitting parameters to one, considerably simplifies the fitting procedure. In this method, the cutoff parameter obtained from the Ginzburg-Landau model was extended over the whole field and temperature ranges. In this case, the effects of the bound states in the vortex cores lead to the Kramer-Pesch effect [67], i.e. delocalization between the vortices [68, 69], nonlocal electrodynamic [58] and nonlinear effects [70] being self-consistently included.

Following the microscopical Eilenberger theory, ξ_h can be found from the fitting of the calculated magnetic field distribution $h_E(\mathbf{r})$ to the Eilenberger - Hao-Clem (EHC) field distribution $h_{EHC}(\mathbf{r})$ [54, 55]

$$h_{EHC}(\mathbf{r}) = \frac{\Phi_0}{S}\sum_{\mathbf{G}}\frac{F(G)e^{i\mathbf{G}\mathbf{r}}}{1+\lambda^2 G^2}, \tag{1}$$

where

$$F(\mathbf{G}) = uK_1(u), \tag{2}$$

where $K_1(u)$ is modified Bessel function, $u = \xi_h G$ and S is the area of the vortex lattice unit cell. It is important to note that ξ_h in Eq. (1) is obtained from solving the Eilenberger equations and does not coincide with the variational parameter ξ_v of the analytical Ginzburg-Landau (AGL) model.

In **chapter 2** and **3** we solve the Eilenberger equations for $s^{\pm}$, s_{++} and $d_{x^2-y^2}$-wave pairing symmetries, fit the solution to Eq. (1) and find the cutoff parameter ξ_h. In this approach all nonlinear and nonlocal effects connected with vortex core and extended quasiclassical states are described by one effective cutoff parameter ξ_h. The nonlocal generalized London equation with separated quasiclassical states was also developed as regards the description of the mixed state in high-T_c superconductors such as $YBa_2Cu_3O_{7-\delta}$ compounds (the Amin-Franz-Affleck (AFA) model) [70, 71]. In this case, fourfold anisotropy arises from d-wave pairing. This theory was applied to the investigation of the flux line lattice (FLL) structures [72] and effective penetration depth measured by μSR experiments [73]. This approach will be considered in **chapter 4**.

2. The cutoff parameter for the field distribution in the mixed states of $s^{\pm}$- and s_{++}-wave pairing symmetries

In this chapter, we consider the model of the iron pnictides, where the Fermi surface is approximated by two cylindrical pockets centered at Γ (hole) and M (electron) points of the

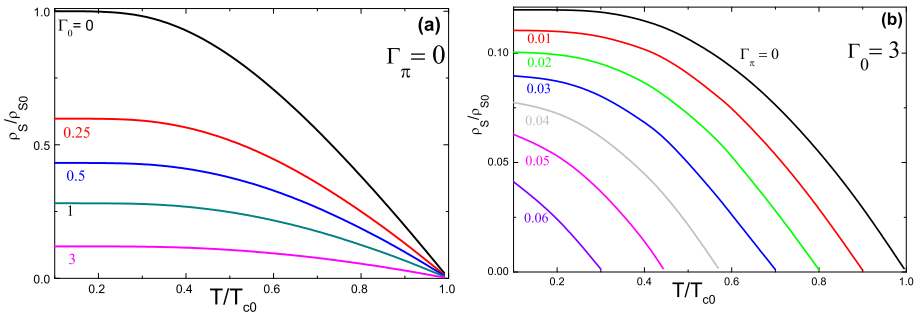

Figure 1. (Color online) The temperature dependence of superfluid density $\rho_S(T)/\rho_{S0}$ at (a) interband scattering rate $\Gamma_\pi = 0$ with different values of intraband scattering Γ_0 and (b) intraband scattering rate $\Gamma_0 = 3$ with different values of interband scattering Γ_π.

Fermi surface, i.e. a two dimensional limit of the five-band model [74]. In Eq. (1) $\lambda(T)$ is the penetration depth in the Meissner state. In this model $\lambda(T)$ is given as

$$\frac{\lambda_{L0}^2}{\lambda^2(T)} = 2\pi T \sum_{\omega_n>0} \frac{\bar{\Delta}_n^2}{\eta_n(\bar{\Delta}_n^2+\omega_n^2)^{3/2}}, \tag{3}$$

where $\lambda_{L0} = (c^2/4\pi e^2 v_F^2 N_0)^{1/2}$ is the London penetration depth at $T = 0$ including the Fermi velocity v_F and the density of states N_0 at the Fermi surface and $\eta_n = 1 + 2\pi(\Gamma_0+\Gamma_\pi)/(\sqrt{\bar{\Delta}_n^2+\omega_n^2})$. Here, $\Gamma_0 = \pi n_i N_F |u_0|^2$ and $\Gamma_\pi = \pi n_i N_F |u_\pi|^2$ are the intra- and interband impurity scattering rates, respectively ($u_{0,\pi}$ are impurity scattering amplitudes with correspondingly small, or close to $\pi = (\pi,\pi)$, momentum transfer). In this work, we investigate the field distribution in the vortex lattice by systematically changing the impurity concentration in the Born approximation, and analyzing the field dependence of the cutoff parameter. In particular, we consider two limits: small $\Gamma^* \ll 1$ (referred to as the "stoichiometric" case) and relatively high $\Gamma^* \geq 1$ ("nonstoichiometric" case). Here, Γ^* is measured in the units of $2\pi T_{c0}$. We consider Γ^* as intraband scattering Γ_0 with constant interband scattering $\Gamma_\pi = 0$.

In Eq. (3), $\bar{\Delta}_n = \Delta(T) - 4\pi\Gamma_\pi\bar{\Delta}_n/\sqrt{\bar{\Delta}_n^2+\omega_n^2}$ for the $s^\pm$ pairing and $\bar{\Delta}_n = \Delta(T)$ for the s_{++} pairing symmetry. The order parameter $\Delta(T)$ in Meissner state is determined by the self-consistent equation

$$\Delta(T) = 2\pi T \sum_{0<\omega_n<\omega_c} \frac{V^{SC}\bar{\Delta}_n}{\sqrt{\bar{\Delta}_n^2+\omega_n^2}}. \tag{4}$$

Experimentally, $\lambda(T)$ can be obtained by radio-frequency measurements [75] and magnetization measurements of nanoparticles [76]. Fig. 1 shows the calculated temperature dependence of the superfluid density $\rho_S(T)/\rho_{S0} = \lambda_{L0}^2/\lambda^2(T)$, with different values of impurity scattering Γ for $s^\pm$-wave pairing symmetry. With the Riccati transformation of the Eilenberger equations, quasiclassical Green functions f and g can be parameterized via functions a and b [77]

$$\bar{f} = \frac{2a}{1+ab}, \quad f^\dagger = \frac{2b}{1+ab}, \quad g = \frac{1-ab}{1+ab}, \tag{5}$$

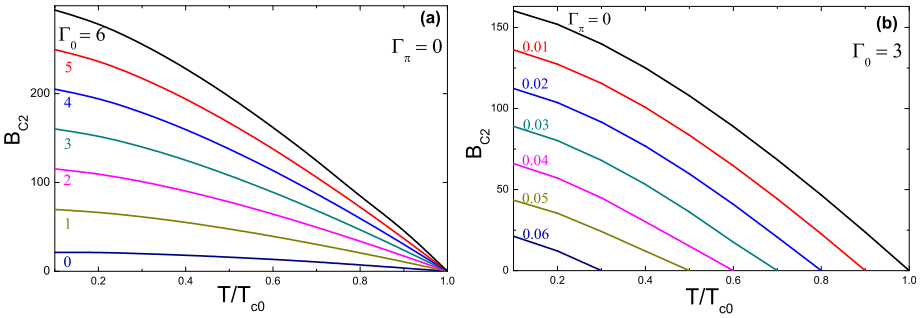

Figure 2. (Color online) (a) The temperature dependence of the upper critical field B_{c2} at interband scattering $\Gamma_\pi = 0$ with different values of intraband scattering values Γ_0. (b) The calculated temperature dependence of B_{c2} at intraband scattering rate $\Gamma_0 = 3$ with different values of interband scattering Γ_π.

satisfying the nonlinear Riccati equations. In Born approximation for impurity scattering we have

$$\mathbf{u}\cdot\nabla a = -a\left[2(\omega_n + G) + i\mathbf{u}\cdot\mathbf{A}_s\right] + (\Delta + F) - a^2(\Delta^* + F^*), \tag{6}$$

$$\mathbf{u}\cdot\nabla b = b\left[2(\omega_n + G) + i\mathbf{u}\cdot\mathbf{A}_s\right] - (\Delta^* + F^*) + b^2(\Delta + F), \tag{7}$$

where $\omega_n = \pi T(2n+1)$, $G = 2\pi\langle g\rangle(\Gamma_0 + \Gamma_\pi) \equiv 2\pi\langle g\rangle\Gamma^*$, $F = 2\pi\langle f\rangle(\Gamma_0 - \Gamma_\pi)$ for $s^{\pm}$ pairing symmetry and $F = 2\pi\langle f\rangle\Gamma^*$ for the s_{++} pairing symmetry. Here, $\mathbf{u}$ is a unit vector of the Fermi velocity. In the new gauge vector-potential $\mathbf{A}_s = \mathbf{A} - \nabla\phi$ is proportional to the superfluid velocity. It diverges as $1/r$ at the vortex center (index s is put to denote its singular nature). The FLL creates the anisotropy of the electron spectrum. Therefore, the impurity renormalization correction in Eqs. (6) and (7), averaged over the Fermi surface, can be reduced to averages over the polar angle θ, i.e. $\langle\ldots\rangle = (1/2\pi)\int\ldots d\theta$.

To take into account the influence of screening the vector potential $\mathbf{A}(\mathbf{r})$ in Eqs. (6) and (7) is obtained from the equation

$$\nabla\times\nabla\times\mathbf{A}_\mathbf{E} = \frac{4}{\kappa^2}\mathbf{J}, \tag{8}$$

where the supercurrent $\mathbf{J}(\mathbf{r})$ is given in terms of $g(\omega_n,\theta,\mathbf{r})$ by

$$\mathbf{J}(\mathbf{r}) = 2\pi T\sum_{\omega_n>0}\int_0^{2\pi}\frac{d\theta}{2\pi}\frac{\hat{\mathbf{k}}}{i}g(\omega_n,\theta,\mathbf{r}). \tag{9}$$

Here $\mathbf{A}$ and $\mathbf{J}$ are measured in units of $\Phi_0/2\pi\xi_0$ and $2ev_F N_0 T_c$, respectively. The spatial variation of the internal field $h(\mathbf{r})$ is determined through

$$\nabla\times\mathbf{A} = \mathbf{h}(\mathbf{r}), \tag{10}$$

where $\mathbf{h}$ is measured in units of $\Phi_0/2\pi\xi_0^2$.

The self-consistent condition for the pairing potential $\Delta(\mathbf{r})$ in the vortex state is given by

$$\Delta(\mathbf{r}) = V^{SC} 2\pi T \sum_{\omega_n>0}^{\omega_c} \int_0^{2\pi} \frac{d\theta}{2\pi} f(\omega_n, \theta, \mathbf{r}), \tag{11}$$

where V^{SC} is the coupling constant and ω_c is the ultraviolet cutoff determining T_{c0} [55]. Consistently throughout our paper energy, temperature, and length are measured in units of T_{c0} and the coherence length $\xi_0 = v_F/T_{c0}$, where v_F is the Fermi velocity. The magnetic field $\mathbf{h}$ is given in units of $\Phi_0/2\pi\xi_0^2$. The impurity scattering rates are in units of $2\pi T_{c0}$. In calculations the ratio $\kappa = \lambda_{L0}/\xi_0 = 10$ is used. It corresponds to $\kappa_{GL} = 43.3$ [77].

To obtain the quasiclassical Green function, the Riccati equations [Eq. (6, 7)] are solved by the Fast Fourier Transform (FFT) method for triangular FLL [55]. This method is reasonable for the dense FLL, discussed in this paper. In the high field the pinning effects are weak and they are not considered in our paper. To study the high field regime we needed to calculate the upper critical field $B_{c2}(T)$. This was found from using the similarity of the considered model to the model of spin-flip superconductors from the equations [78]

$$\ln(\frac{T_{c0}}{T}) = 2\pi T \sum_{n\geq 0} [\omega_n^{-1} - 2D_1(\omega_n, B_{c2})], \tag{12}$$

where

$$D_1(\omega_n, B_{c2}) = J(\omega_n, B_{c2}) \times [1 - 2(\Gamma_0 - \Gamma_\pi) J(\omega_n, B_{c2})]^{-1}, \tag{13}$$

$$J(\omega_n, B_{c2}) = (\frac{4}{\pi B_{c2}})^{1/2} \times \int_0^\infty dy \exp(-y) \arctan[\frac{(B_{c2}y)^{1/2}}{\alpha}], \tag{14}$$

where $\alpha = 2(\omega_n + \Gamma_0 + \Gamma_\pi)$.

Fig. 2 shows $B_{c2}(T)$ dependences at (a) $\Gamma_\pi = 0$, $\Gamma_0 = 0, 1, 2, 3, 4, 5, 6$ and (b) $\Gamma_0 = 3$, $\Gamma_\pi = 0.01, 0.02, 0.03, 0.04, 0.05, 0.06$ calculated from Eqs. (12-14). In Fig. 2 the different influence of the intraband and interband scattering on $B_{c2}(T)$ dependence can be seen. The $B_{c2}(T)$ curve increases with Γ_0 (ξ_{c2} decreases with Γ_0), but Γ_π results in decreasing $B_{c2}(T)$ (increasing of ξ_{c2}).

Fig. 3 (a) shows magnetic field dependence $\xi_h(B)$ in reduced units at $T/T_{c0} = 0.5$ for the $s^\pm$ pairing with $\Gamma_0 = 3$, $\Gamma_\pi = 0.02$ and $\Gamma_0 = 0.5$, $\Gamma_\pi = 0.03$ and "clean" case (solid lines) and for the s_{++} pairing with Γ^*= 0.5 and $\Gamma^* = 3$ (dotted lines). The dashed line shows the analytical solution of the AGL theory [63]

$$\xi_v = \xi_{c2}(\sqrt{2} - \frac{0.75}{\kappa_{GL}})(1 + b^4)^{1/2}[1 - 2b(1-b)^2]^{1/2}. \tag{15}$$

This dependence with ξ_{c2} as a fitting parameter is often used for the description of the experimental μSR results [56, 79]. As can be seen from Fig. 3 (a), the magnetic field dependence of ξ_h/ξ_{c2} is nonuniversal because it depends not only on B/B_{c2} (as in the AGL theory, dashed line in Fig. 3 (a)), but also on interband and intraband impurity scattering parameters. In the cases where $\Gamma_0 = \Gamma_\pi = 0$, the results are the same for $s^\pm$ and s_{++} pairing symmetries. We indicated that this curve is "clean" one. In this figure, the case $\Gamma_0 \gg \Gamma_\pi$ is considered

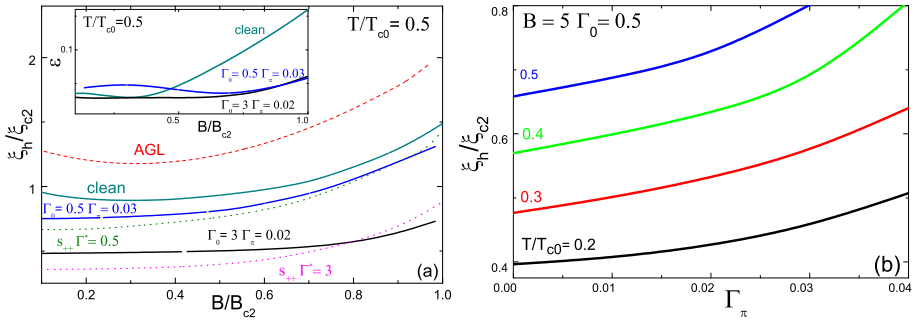

Figure 3. (Color online) (a) The magnetic field dependence of ξ_h/ξ_{c2} for superconductors with impurity scattering. The solid lines represent our solution of Eilenberger equations at $T/T_{c0} = 0.5$ for "clean" case ($\Gamma_0 = \Gamma_\pi = 0$) and $s^{\pm}$ model ($\Gamma_0 = 0.5$, $\Gamma_\pi = 0.03$ and $\Gamma_0 = 3$, $\Gamma_\pi = 0.02$). The dotted lines show result for s_{++} model ($\Gamma^* = 0.5$ and $\Gamma^* = 3$). Dashed line demonstrates the result of the AGL theory for ξ_v from Eq. 15. The inset shows the magnetic field dependence of mean square deviation of the h_{EHC} distribution from the Eilenberger distribution normalized by the variance of the Eilenberger distribution, ε, for $T/T_{c0} = 0.5$ at $\Gamma_0 = \Gamma_\pi = 0$ ("clean"); $\Gamma_0 = 3$, $\Gamma_\pi = 0.02$ and $\Gamma_0 = 0.5$, $\Gamma_\pi = 0.03$. (b) The interband scattering Γ_π dependence of ξ_h/ξ_{c2} at different temperatures T/T_{c0} (intraband scattering $\Gamma_0 = 0.5$ and $B = 5$) for the $s^{\pm}$ pairing.

and the value of ξ_h is reduced considerably in comparison with the clean case. One can compare the observed behavior with that in s_{++} pairing model. In s_{++} pairing symmetry the intraband and interband scattering rates act in a similar way and ξ_h/ξ_{c2} decreases always with impurity scattering. In contrast, in $s^{\pm}$ model $\xi_h/\xi_{c2}(B/B_{c2})$ dependences show different forms of behavior with Γ_π. Here, ξ_h/ξ_{c2} increases with Γ_π at $B/B_{c2} < 0.8$ and decreases at higher fields, i.e. the curves become more flattened. A crossing point appears in the dependences $\xi_h/\xi_{c2}(B/B_{c2})$ for $s^{\pm}$ and s_{++} pairing. We also calculated the magnetic field dependence of mean square deviation of h_{EHC} distribution of the magnetic field from the Eilenberger distribution normalized by the variance of the Eilenberger distribution $\varepsilon = \sqrt{\overline{(h_E - h_{EHC})^2}/\overline{(h_E - B)^2}}$, where $\overline{\cdots}$ is the average over a unit vortex cell. The inset to Fig. 3 (a) demonstrates $\varepsilon(B)$ dependence for $T/T_{c0} = 0.5$ at $\Gamma_0 = 0$, $\Gamma_\pi = 0$; $\Gamma_0 = 3$, $\Gamma_\pi = 0.02$ and $\Gamma_0 = 0.5$, $\Gamma_\pi = 0.03$. From this figure, it can be seen that the accuracy of effective London model is deteriorating as the magnetic field increases; however, in superconductors with impurity scattering the accuracy is below 6% even when it is close to the second critical field (the inset to Fig. 3 (a)).

In Fig. 3 (b), the interband scattering Γ_π dependences of ξ_h are presented in low fields for the $s^{\pm}$ pairing at different temperatures T. As can be seen ξ_h/ξ_{c2} increases with the interband scattering rate Γ_π. Strong decreasing of ξ_h/ξ_{c2} with a decrease in the temperature can be explained by the Kramer-Pesch effect [67]. It should be noted that the normalization constant ξ_{c2} increases with Γ_π because Γ_π suppress T_c similar to superconductors with spin-flip scattering (violation of the Anderson theorem). Thus, the rising ξ_h/ξ_{c2} implies more strong growth of ξ_h than ξ_{c2} (from GL theory one can expect $\xi_h/\xi_{c2} = Const$). Qualitatively, it can be explained by the strong temperature dependence of $\xi_h(B, T/T_c)$, which is connected to the Kramer-Pesch effect [67]. Increasing Γ_π results in suppression of T_c, i.e. effective increasing of T and $\xi_h(T/T_c)$. $\xi_{c2}(T/T_c)$ has not such a strong T_c dependence, thus leading to the increasing of the ratio ξ_h/ξ_{c2} with Γ_π.

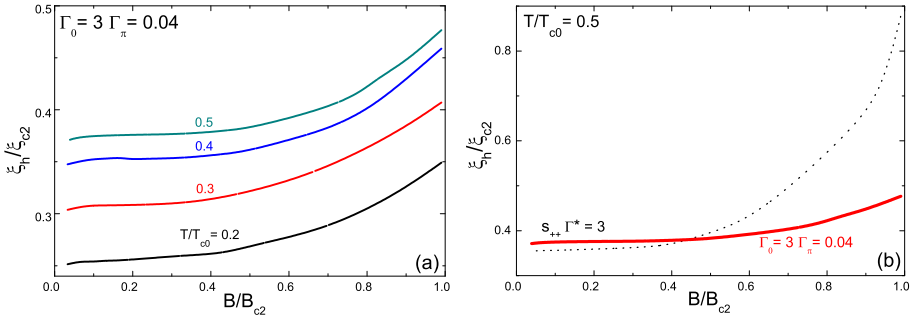

Figure 4. (Color online) (a) The magnetic field dependence of cutoff parameter ξ_h/ξ_{c2} at different temperatures ($T/T_{c0} = 0.2, 0.3, 0.4, 0.5$) for $s^{\pm}$ pairing with $\Gamma_0 = 3$, $\Gamma_\pi = 0.04$. (b) The magnetic field dependence of ξ_h/ξ_{c2} for $s^{\pm}$ model ($\Gamma_0 = 3$, $\Gamma_\pi = 0.04$, solid line) and s_{++} model ($\Gamma^* = 3$, dotted line) at $T/T_{c0} = 0.5$.

The superfluid density in iron pnictides often shows a power law dependence with theexponent, which is approximately equal to two at low temperatures [39, 74]. This law was explained by $s^{\pm}$ model with parameters $\Gamma_0 = 3$ and $\Gamma_\pi = 0.04 - 0.06$. Fig. 4 (a) shows $\xi_h/\xi_{c2}(B/B_{c2})$ dependence with $\Gamma_0 = 3$ and $\Gamma_\pi = 0.04$ at different temperatures. All curves demonstrate rising behavior with values much less than one in the whole field range, i.e. they are under the AGL curve of ξ_v. The small value of the cutoff parameter was observed in iron pnictide $BaFe_{1.82}Co_{0.18}As$, where $\xi_h/\xi_{c2}(\sim 0.4) < 1$ [80]. Fig. 4 (b) shows $\xi_h/\xi_{c2}(B/B_{c2})$ for $\Gamma_0 = 3$, $\Gamma_\pi = 0.04$ ($s^{\pm}$ pairing) and $\Gamma^* = 3$ (s_{++} pairing). It can be seen from the graph that ξ_h/ξ_{c2} is strongly suppressed in $s^{\pm}$ pairing with comparison to the s_{++} pairing. This can be explained by the fact that in superconductors, without interband pair breaking, the increase in high field is connected with the field-dependent pair breaking, as the upper critical field is approached. The physics of unconventional superconductors depends on impurity pair breaking and introducing characteristic field B^* in the field dependence by the substitution $B/B_{c2} \to (B + B^*(\Gamma_\pi))/B_{c2}(\Gamma_\pi)$. The crossing point between $s^{\pm}$ and s_{++} curves depends on Γ_π and it shifts to the lower field in comparison with case $\Gamma_\pi = 0.02$ shown in Fig. 3 (a).

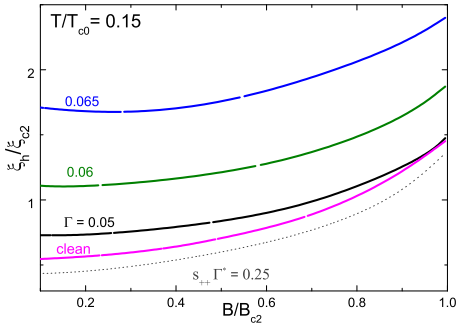

Figure 5. (Color online) The magnetic field dependence of the cutoff parameter at $T/T_{c0} = 0.15$ with the same values of intraband Γ_0 and interband Γ_π scattering rate Γ ($\Gamma = 0$ for "clean" case and $\Gamma = 0.05, 0.06, 0.065$ for the $s^{\pm}$ pairing). Dotted line shows result for s_{++} model ($\Gamma^* = 0.25$).

The case of weak intraband scattering was also studied. This case can be realized in stoichiometrical pnictides such as LiFeAs. Fig. 5 presents the magnetic field dependence of ξ_h/ξ_{c2} with scattering parameters $\Gamma_0 = \Gamma_\pi = \Gamma$ equal to 0, 0.05, 0.06 and 0.065 at $T/T_{c0} = 0.15$. The dotted line shows the result for s_{++} model ($\Gamma^* = 0.25$). The $\xi_h(B)$ dependence shifts upward from the "clean" curve and has a higher values in $s^{\pm}$ model. In contrast, the ξ_h/ξ_{c2} curve shifts downward with impurity scattering in s_{++} model. The high values of ξ_h observed in μSR measurements in LiFeAs [81] supports the $s^{\pm}$ pairing.

3. The cutoff parameter in the mixed state of $d_{x^2-y^2}$-wave pairing symmetry

A nontrivial orbital structure of the order parameter, in particular the presence of the gap nodes, leads to an effect in which the disorder is much richer in $d_{x^2-y^2}$-wave superconductors than in conventional materials. For instance, in contrast to the s-wave case, the Anderson theorem does not work, and nonmagnetic impurities exhibit a strong pair-breaking effect. In addition, a finite concentration of disorder produces a nonzero density of quasiparticle states at zero energy, which results in a considerable modification of the thermodynamic and transport properties at low temperatures. For a pure superconductor in a d-wave-like state at temperatures T well below the critical temperature T_c, the deviation $\Delta\lambda$ of the penetration depth from its zero-temperature value $\lambda(0)$ is proportional to T. When the concentration n_i of strongly scattering impurities is nonzero, $\Delta\lambda \propto T^n$, where $n = 2$ for $T < T^* \ll T_c$ and $n = 1$ for $T^* < T \ll T_c$ [24]. Unlike s-wave superconductor, impurity scattering suppresses both the transition temperature T_c and the upper critical field $H_{c2}(T)$ [82].

The presence of the nodes in the superconducting gap can also result in unusual properties of the vortex state in $d_{x^2-y^2}$-wave superconductors. At intermediate fields $H_{c1} < H \ll H_{c2}$, properties of the flux lattice are determined primarily by the superfluid response of the condensate, i.e., by the relation between the supercurrent $\vec{j}$ and the superfluid velocity $\vec{v}_s$. In conventional isotropic strong type-II superconductors, this relation is to a good approximation that of simple proportionality,

$$\vec{j} = -e\rho_s\vec{v}_s, \tag{16}$$

where ρ_s is a superfluid density. More generally, however, this relation can be both nonlocal and nonlinear. The concept of nonlocal response dates is a return to the ideas of Pippard [83] and is related to the fact that the current response must be averaged over the finite size of the Cooper pair given by the coherence length ξ_0. In strongly type-II materials the magnetic field varies on a length scale given by the London penetration depth λ_0, which is much larger than ξ_0 and, therefore, nonlocality is typically unimportant unless there exist strong anisotropies in the electronic band structure [84]. Nonlinear corrections arise from the change of quasiparticle population due to superflow which, to the leading order, modifies the excitation spectrum by a quasiclassical Doppler shift [85]

$$\varepsilon_k = E_k + \vec{v}_f\vec{v}_s, \tag{17}$$

where $E_k = \sqrt{\epsilon_k^2 + \Delta_k^2}$ is the BCS energy. Once again, in clean, fully gapped conventional superconductors, this effect is typically negligible except when the current approaches the pair breaking value. In the mixed state, this happens only in the close vicinity of the vortex cores that occupy a small fraction of the total sample volume at fields well below H_{c2}. The situation changes dramatically when the order parameter has nodes, such as in $d_{x^2-y^2}$ superconductors.

Nonlocal corrections to Eq. (16) become important for the response of electrons with momenta on the Fermi surface close to the gap nodes, even in strongly type-II materials. This can be understood by realizing that the coherence length, being inversely proportional to the gap [85], becomes very large close to the node and formally diverges at the nodal point. Thus, quite generally, there exists a locus of points on the Fermi surface where $\xi \gg \lambda_0$ and the response becomes highly nonlocal. This effect was first discussed in Refs. [72, 86] in the mixed state. Similarly, the nonlinear corrections become important in a d-wave superconductors. Eq. (17) indicates that finite areas of gapless excitations appear near the node for arbitrarily small v_s.

Low temperature physics of the vortex state in s-wave superconductors is connected with the nature of the current-carrying quantum states of the quasiparticles in the vortex core (formed due to particle-hole coherence and Andreev reflection [87]). The current distribution can be decomposed in terms of bound states and extended states contributions [88]. Close to the vortex core, the current density arises mainly from the occupation of the bound states. The effect of extended states becomes important only at distances larger than the coherence length. The bound states and the extended states contributions to the current density have opposite signs. The current density originating from the bound states is paramagnetic, whereas extended states contribute a diamagnetic term. At distances larger than the penetration depth, the paramagnetic and diamagnetic parts essentially cancel out each other, resulting in exponential decay of the total current density. The vortex core structure in the d-wave superconductors can be more complicated because there are important contributions coming from core states, which extend far from the vortex core into the nodal directions and significantly effect the density of states at low energy [89]. The possibility of the bound states forming in the vortex core of d-wave superconductors was widely discussed in terms of the Bogoliubov-de Gennes equation. For example, Franz and Teŝanoviĉ claimed that there should be no bound states [90]. However, a considerable number of bound states were found in Ref.[91] which were localized around the vortex core. Extended states, which are rather uniform, for $|E| < \Delta$ where E is the quasiparticle energy and Δ is the asymptotic value of the order parameter, were also found far away from the vortex. In the problem of the bound states, the conservation of the angular momentum around the vortex is important. In spite of the strict conservation of the angular momentum it is broken due to the fourfold symmetry of $\Delta(k)$, however, the angular momentum is still conserved by modulo 4, and this is adequate to guarantee the presence of bound states.

Taking into account all these effects, the applicability of EHC theory regarding the description of the vortex state in $d_{x^2-y^2}$-wave superconductors is not evident *apriori*. In this chapter, we numerically solve the quasiclassical Eilenberger equations for the mixed state of a $d_{x^2-y^2}$-wave superconductor for the pairing potential $\Delta(\theta, \mathbf{r}) = \Delta(\mathbf{r}) \cos(2\theta)$, where θ is the angle between the $\mathbf{k}$ vector and the a axis (or x axis). We check the applicability of Eq. (1) and find the cutoff parameter ξ_h. The anisotropic extension of Eq. (1) to Amin-Franz-Affleck will be discussed in chapter 4.

To consider the mixed state of a d-wave superconductor we take the center of the vortex as the origin and assume that the Fermi surface is isotropic and cylindrical. The Riccatti equations for $d_{x^2-y^2}$-wave superconductivity are [92]

$$\mathbf{u} \cdot \nabla a = -a\left[2(\omega_n + G) + i\mathbf{u} \cdot \mathbf{A}_s\right] + \Delta - a^2\Delta^*, \tag{18}$$

$$\mathbf{u} \cdot \nabla b = b\left[2(\omega_n + G) + i\mathbf{u} \cdot \mathbf{A}_s\right] - \Delta^* + b^2\Delta, \tag{19}$$

where $G = 2\pi \langle g \rangle \Gamma$ with d-wave pairing potential $\Delta(r)$

$$\Delta(\theta, \mathbf{r}) = V^{SC}_{d_{x^2-y^2}} 2\pi T \cos(2\theta) \sum_{\omega_n > 0}^{\omega_c} \int_0^{2\pi} \frac{d\bar{\theta}}{2\pi} f(\omega_n, \bar{\theta}, \mathbf{r}) cos(2\bar{\theta}), \tag{20}$$

where $V^{SC}_{d_{x^2-y^2}}$ is a coupling constant in the $d_{x^2-y^2}$ pairing channel. The obtained solution is fitted to Eq. (1) giving the value of cutoff parameter ξ_h for $d_{x^2-y^2}$-wave pairing symmetry.

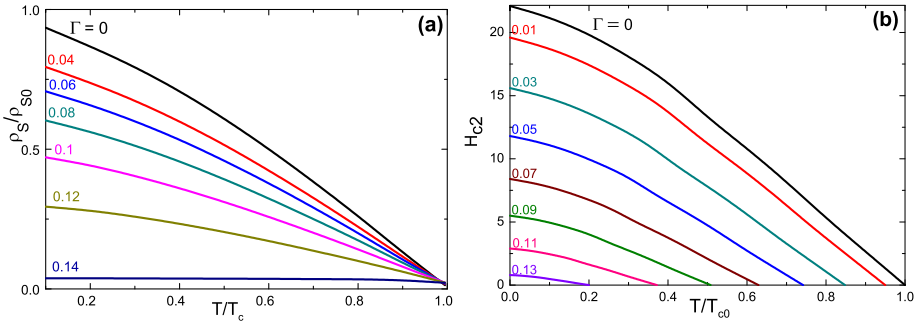

Figure 6. (Color online) (a) The temperature dependence of superfluid density $\rho_S(T)/\rho_{S0}$ with different values of impurity scattering Γ. (b) The temperature dependence of the upper critical field B_{c2} with different values of impurity scattering Γ.

In $d_{x^2-y^2}$-wave superconductor $\lambda(T)$ in Eq. (1) is given as [85]

$$\frac{\lambda^2_{L0}}{\lambda^2(T)} = 2\pi T \oint \frac{d\theta}{2\pi} \sum_{\omega_n > 0} \frac{|\tilde{\Delta}(\theta)|^2}{(\tilde{\omega}_n^2 + |\tilde{\Delta}(\theta)|^2)^{3/2}}, \tag{21}$$

where

$$\tilde{\omega}_n = \omega_n + \Gamma \langle \frac{\tilde{\omega}_n}{\sqrt{\tilde{\omega}_n^2 + |\tilde{\Delta}(\vec{p}_f^{\,\prime}; \omega_n)|^2}} \rangle_{\vec{p}_f^{\,\prime}}, \tag{22}$$

$$\tilde{\Delta}(\vec{p}_f; \omega_n) = \Delta(\vec{p}_f) + \Gamma \langle \frac{\tilde{\Delta}(\vec{p}_f^{\,\prime}; \omega_n)}{\sqrt{\tilde{\omega}_n^2 + |\tilde{\Delta}(\vec{p}_f^{\,\prime}; \omega_n)|^2}} \rangle_{\vec{p}_f^{\,\prime}}, \tag{23}$$

$$\Delta(\vec{p}_f) = \int d\vec{p}_f^{\,\prime} V(\vec{p}_f, \vec{p}_f^{\,\prime}) \pi T \sum_{\omega_n}^{|\omega_n| < \omega_c} \frac{\tilde{\Delta}(\vec{p}_f^{\,\prime})}{\sqrt{\tilde{\omega}_n^2 + |\tilde{\Delta}(\vec{p}_f^{\,\prime})|^2}}. \tag{24}$$

Because of the symmetry of $d_{x^2-y^2}$-wave pairing the impurity induced corrections for the pairing potential in Eq. (23) are zero and $\tilde{\Delta} = \Delta$. This is different from the $s^{\pm}$- and s_{++} cases, where the corrections are not zero. Fig. 6 (a) shows the calculated temperature dependence of the superfluid density $\rho_S(T)/\rho_{S0} = \lambda^2_{L0}/\lambda^2(T)$ with different values of impurity scattering Γ for $d_{x^2-y^2}$-wave pairing symmetry.

To study high the field regime we need to calculate the upper critical field $B_{c2}(T)$. For $d_{x^2-y^2}$-wave $B_{c2}(T)$ is given as [82]

$$\ln(\frac{T}{T_c}) - \Psi(\frac{1}{2} + \frac{v}{2t_c}) + \Psi(\frac{1}{2} + \frac{v}{2t}) = \frac{3}{2} \int_0^{\infty} \frac{du}{shu} \int_0^1 dz(1 - z^2)[e^{-x}(1 - 2xc)^{-1}] e^{-\frac{v}{t}u}, \tag{25}$$

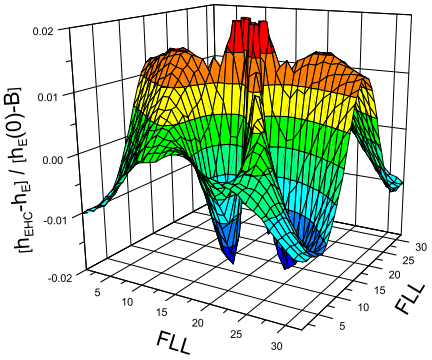

Figure 7. (Color online) Normalized differences between the fields calculated with the London model and the Eilenberger equation for $d_{x^2-y^2}$-wave pairing with $\Gamma = 0.03$, $B/B_{c2} = 0.1$ and $T/T_{c0} = 0.3$.

$$c[\ln(\frac{T}{T_c}) - \Psi(\frac{1}{2} + \frac{v}{2t_c}) + \Psi(\frac{1}{2} + \frac{v}{2t})] =$$

$$= \frac{3}{2}\int_0^\infty \frac{du}{shu} x \int_0^1 dz |(1-z^2)[e^{-x}(-x + c(1-4x+2x^2)) - c]e^{-\frac{v}{t}u}, \qquad (26)$$

where $v = 2\Gamma$, $t = T/T_{c0}$, $t_c = T_c/T_{c0}$ and $x = \rho u^2(1-z^2)$, $\rho = B/(4\pi t)^2$. Fig. 6 (b) depicts the temperature dependence of the upper critical field B_{c2} with different values of impurity scattering Γ. Figs. 6 (a) and (b) are similar to those in $s^{\pm}$-wave superconductors. T_c is suppressed by impurity scattering resulting in the same expressions for $s^{\pm}$ and d-wave superconductors with replacing $\Gamma_\pi \to \Gamma/2$.

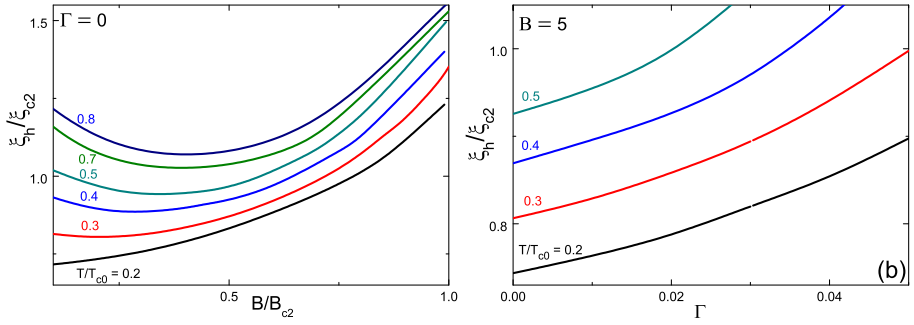

Figure 8. (Color online) (a) The magnetic field dependence of the cutoff parameter ξ_h/ξ_{c2} with different temperatures ($T/T_{c0} = 0.2, 0.3, 0.4, 0.5, 0.7, 0.8$) for $d_{x^2-y^2}$ pairing with $\Gamma = 0$. (b) The impurity scattering Γ dependence of ξ_h/ξ_{c2} at different temperatures for $d_{x^2-y^2}$ pairing with $B = 5$.

Fig. 7 shows the normalized differences between the fields calculated with the London model and the Eilenberger equations for $d_{x^2-y^2}$-wave pairing symmetry for the values of $\Gamma = 0.03$, $B/B_{c2} = 0.1$ and $T/T_{c0} = 0.3$. The accuracy of the fitting is better than 2%.

Fig. 8 (a) demonstrates the magnetic field dependence of cutoff parameter ξ_h/ξ_{c2} at different temperatures ($T/T_{c0} = 0.2, 0.3, 0.4, 0.5, 0.7, 0.8$) for $d_{x^2-y^2}$ pairing with $\Gamma = 0$. Fig. 8 (b) shows the impurity scattering Γ dependence of ξ_h/ξ_{c2} at different temperatures for $d_{x^2-y^2}$

pairing with $B = 5$. For clean superconductors (Fig. 8 (a)) ξ_h/ξ_{c2} has a minimum in its field dependence similar to usual s-wave superconductors [93]. However, this ratio decreases with temperature due to Kramer-Pesch effect. It was demonstrated theoretically and experimentally that the low energy density of states $N(E)$ is described by the same singular V-shape form $N(E) = N_0(H) + \alpha|E| + O(E^2)$ for all clean superconductors in a vortex state, irrespective of the underlying gap structure [94]. This explains the similarity in the behavior between s- and d-wave pairing symmetries.

The difference between pairing symmetries reveals itself in impurity scattering dependence ξ_h/ξ_{c2}. In s_{++} symmetry ξ_h/ξ_{c2} always decreases with impurity scattering rate Γ (Fig. 3 (a)), in $s^{\pm}$ symmetry its behavior depends on the field range and relative values of intraband and interband impurity scattering rates: it can be a decreasing function of Γ_π (Fig. 4 (b)) or an increasing function of Γ_π (Fig. 3 (b)). In d-wave superconductors ξ_h/ξ_{c2} always increases with Γ (Fig. 8 (b)) similar to the case of $s^{\pm}$ symmetry with $\Gamma_0 = \Gamma_\pi$ (Fig. 5). This can be understood from the comparison of the Ricatti equations of the $s^{\pm}$ and d-wave pairing. In both cases the renormalization factor $F = 0$ due to a cancelation of the intraband and interband impurity scattering rates in $s^{\pm}$ pairing or symmetry reason $\langle f \rangle = 0$ for d-wave pairing.

4. The quasiclassical approach to the Amin-Franz-Affleck model and the effective penetration depth in the mixed state in $d_{x^2-y^2}$-wave pairing symmetry

In this chapter, we construct a model where the nonlinear corrections arising from the Doppler energy shift of the quasiparticle states by the supercurrent [85] and effects of the vortex core states are described by an effective cutoff function. Nonlocal effects of the extended quasiparticle states are included in our model explicitly, i. e. instead of $\lambda(T)$ in Eq. (1) we use an analytically obtained anisotropic electromagnetic response tensor [70, 72, 73]. Because the nonlocal effects are assumed to be effective in clean superconductors we limit our consideration to the case $\Gamma = 0$.

For a better comparison with the nonlocal generalized London equation (NGLE) and the AGL theory we used another normalization of the cutoff parameter in Eq. (1), $u = k_1\sqrt{2}\xi_{BCS}G$. This form of $F(G)$ correctly describes the high temperature regime. We compare our results with those obtained from the NGLE theory in a wide field and temperature range considering k_1 as the fitting parameter.

The magnetic field distribution in the mixed state in the NGLE approximation is given by [72]

$$h_{NGLE}(\mathbf{r}) = \frac{\Phi_0}{S}\sum_{\mathbf{G}}\frac{F(G)e^{i\mathbf{G}\mathbf{r}}}{1 + L_{ij}(\mathbf{G})G_iG_j}, \tag{27}$$

where

$$L_{ij}(\mathbf{G}) = \frac{Q_{ij}(\mathbf{G})}{\det\hat{\mathbf{Q}}(\mathbf{G})}. \tag{28}$$

The anisotropic electromagnetic response tensor is defined by

$$Q_{ij}(\mathbf{G}) = \frac{4\pi T}{\lambda_{L0}^2}\sum_{\omega_n>0}\int_0^{2\pi}\frac{d\theta}{2\pi}\frac{\Delta(\theta)^2\vartheta_{Fi}\vartheta_{Fj}}{\sqrt{\omega_n^2 + |\Delta(\theta)^2|}(\omega_n^2 + |\Delta(\theta)^2| + \gamma_{\mathbf{G}}^2)}, \tag{29}$$

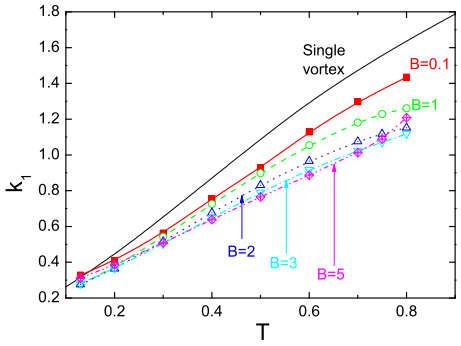

Figure 9. (Color online) The temperature dependence of the coefficient k_1 in the NGLE model obtained at $\kappa = 10$ and $B = 0.1, 1, 2, 3, 5$ from a fitting made with the solution of the Eilenberger equations.

where $\gamma_{\mathbf{G}} = \mathbf{v}_F \cdot \mathbf{G}/2$. In Eq. (29) the term with $\gamma_{\mathbf{G}}$ describes the nonlocal correction to the London equation. Putting $\gamma_{\mathbf{G}} = 0$ we obtain the London result $L_{ij}(\mathbf{G}) = \lambda(T)^2\delta_{ij}$. We use the same shape of the cutoff function as in Eq. (1) but the values of the cutoff parameters are different because of fitting them to the various field distributions. In presentation of h_{NGLE} the anisotropy effects of the Eilenberger theory remain.

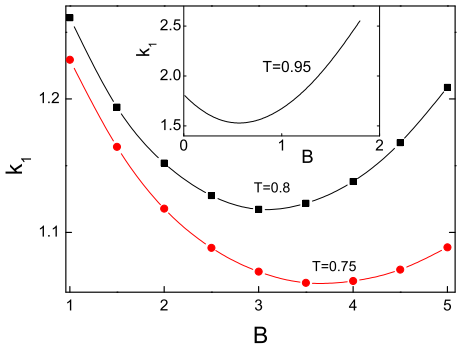

Figure 10. (Color online) Field dependence of k_1 at $T = 0.75$ and 0.8 obtained from the fitting to the Eilenberger equations. The inset shows $k_1(B)$ calculated from the Hao-Clem theory at $T = 0.95$.

Fig. 9 shows the $k_1(T)$ dependence in the NGLE model obtained at $\kappa = 10$ and $B = 0.1, 1, 2, 3, 5$ from the fitting to the solution of the Eilenberger equations. As can be seen from Fig. 9 the coefficient k_1 is strongly reduced at low temperatures. This is a reminiscent of the Kramer-Pesch result for s-wave superconductors (shrinking of the vortex core with decreasing temperature) [95]. It is also found that k_1 is a decreasing function of B. This can be explained by reduction of the vortex core size by the field [68]. The topmost curve in Fig. 9 gives the values of k_1 calculated for a single vortex [96]. At high temperatures the Ginzburg-Landau theory can be applied. Using the values of the parameters of this theory for d-wave superconductors [97] $\xi_{GL} = \xi_{BCS}\pi/\sqrt{3}$ is obtained. A variational approach of the Ginzburg-Landau equations for the single vortex [62] gives $k_1 = \pi/\sqrt{3} \approx 1.81$ is in reasonable agreement with the high temperature limit of k_1 for a single vortex in Fig. 9. Another interesting observation is the nonmonotonic behavior of $k_1(B)$ in low fields at high

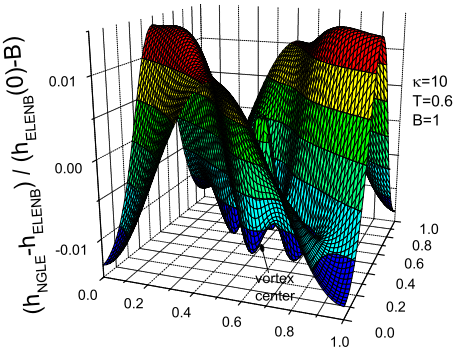

Figure 11. (Color online) Normalized differences between the fields calculated with the London model (NGLE) and the Eilenberger equation (ELENB) for $B = 1$ and $T = 0.6$. The scales of lengths are those of the flux line lattice unit vectors.

temperatures. Fig. 10 depicts the field dependence of k_1 at $T = 0.75$ and 0.8 showing a minimum which moves to lower fields with increasing of the temperature. This result agrees qualitatively with the Hao-Clem theory [63] which also predicts a minimum in the $k_1(B)$ dependence. This is demonstrated in the inset to Fig. 10, where $k_1(B)$ is shown at $T = 0.95$.

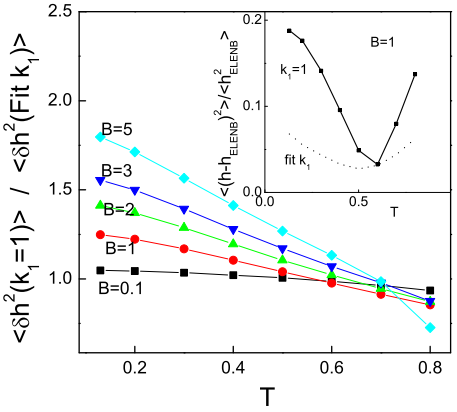

Figure 12. (Color online) Temperature dependence of the ratio of the second moment of the magnetic field distributions obtained from the NGLE model with the fixed and fitted parameter k_1 (see the text below). The inset shows the mean-square deviation of the magnetic field distribution from the origin for parameter k_1 set to unity (solid line) and fitted (dotted line).

The quality of the fitting can be seen from Fig. 11 where the normalized difference between the fields calculated in the NGLE model and the Eilenberger equations at $B = 1$, $T = 0.6$ and $\kappa = 10$ is shown. The accuracy of the fitting is about 1 percent. Thus, there is only a little improvement in the Eilenberger equations fitting to NGLE theory in comparison with local London theory (Eq. (1)). The similarity of the field and temperature dependences of the cutoff parameter in these theories are shown in Fig. 9 and Fig. 10.

To show the influence of the magnetic field and temperature on k_1 dependence, we calculate the values of $\langle \delta h^2_{NGLE} \rangle$ using the field distribution obtained in the Eq. 27. Fig. 12 shows

the temperature dependence of the ratio $\langle \delta h^2_{NGLE} \rangle$ with the cutoff parameter obtained from the solution of the Eilenberger equations to that with $k_1 = 1$. From the data presented in Fig. 12, it can be sen that this ratio deviates considerably from unity when the temperature is lowered, which points to the importance of the proper determination of the value for the cutoff parameter. For the magnetic field distribution, obtained from solving the NGLE, we also calculate the mean-square deviation of this distribution from the origin (the Eilenberger equations solution). The inset demonstrates this deviation for fixed and fitted parameter k_1.

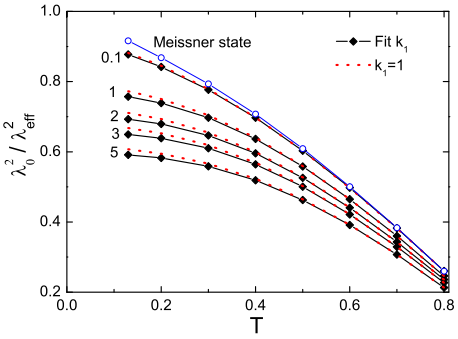

Figure 13. (Color online) The ratio of λ_0 to λ_{eff} calculated from the NGLE equation with $k_1 = 1$ and k_1 from Fig. 9.

This consideration proves that the nonlocal generalized London model with $h_{NGLE}(\mathbf{r})$ distribution also needs the properly determined cutoff parameter k_1, *i.e.* introducing only nonlocal extended electronic states does not allow the avoidance of the problem of vortex core solving.

In the analysis of the experimental μSR and SANS data the field dependent penetration depth $\lambda_{eff}(B)$ is often introduced [56]. It has physical sense even if it is not dependent on the core effects, *i.e.* it should be an invariant of the cutoff parameter. One such way of doing this was suggested in the AFA model [70, 73]:

$$\frac{\lambda_{eff}}{\lambda} = \left(\frac{|\delta h_0^2|}{|\delta h^2_{NGLE}|}\right)^{1/4}. \tag{30}$$

Here, $|\delta h_0^2|$ is the variance of the magnetic field $h_0(\mathbf{r})$ obtained by applying the ordinary London model with the same average field B and λ and with the same cutoff parameter as in the field distribution $h_{NGLE}(\mathbf{r})$.

In Fig. 13 establishes the temperature dependence of the ratio $\lambda_0^2/\lambda_{eff}^2$ calculated from the h_{NGLE} distribution with $k_1 = 1$ and with Fit k_1 from the solution of Eilenberger equations for the different field value. The obtained $\lambda_{eff}(B)$ dependences are quite similar in these cases. The low-field result ($B/B_0 = 0.1$) for λ_{eff} is close to $\lambda(T)$ in the Meissner state. This demonstrates that λ_{eff} is determined by a large scale of the order of FLL period and is not very sensitive to details of the microscopical core structure and the cutoff parameter [98]. The AFA model was originally developed in order to explain the structural transition in FLL in d-wave superconductors where anisotropy and nonlocal effects arise from nodes in the gap at the Fermi surface and the appearance there of the long extending electronic states [72].

The obtained anisotropy of superconducting current around the single vortex in AFA theory agrees reasonably with that found from the Eilenberger equations [96]. Extending electronic states also results in the observed field dependent flattening of $\lambda_{eff}(B)$ at low temperatures [73]. Thus, our microscopical consideration justifies the phenomenological AFA model and the separation between localized and extended states appears to be quite reasonable.

5. Conclusions

The core structure of the vortices is studied for $s^{\pm}$, $d_{x^2-y^2}$ symmetries (connected with interband and intraband antiferromagnetic spin fluctuation mechanism, respectively) and s_{++} symmetry (mediated by moderate electron-phonon interaction due to Fe-ion oscillation and the critical orbital fluctuation) using Eilenberger approach and compared with the experimental data for iron pnictides. It is assumed [99] that the nodeless $s^{\pm}$ pairing state is realized in all optimally-doped iron pnictides, while nodes in the gap are observed in the over-doped KFe_2As_2 compound, implying a $d_{x^2-y^2}$-wave pairing state, there are also other points of view [10, 13]. The stoichiometrical LiFeAs, without antifferomagmetic ordering, is considered as a candidate for the implementation of the s_{++} symmetry. Different impurity scattering rate dependences of cutoff parameter ξ_h are found for $s^{\pm}$ and s_{++} cases. In the nonstoichiometric case, when intraband impurity scattering (Γ_0) is much larger than the interband impurity scattering rate (Γ_π) the ξ_h/ξ_{c2} ratio is less in $s^{\pm}$ symmetry. When $\Gamma_0 \approx \Gamma_\pi$ (stoichiometric case) opposite tendencies are found, in $s^{\pm}$ symmetry the ξ_h/ξ_{c2} rises above the "clean" case curve ($\Gamma_0 = \Gamma_\pi = 0$) while it decreases below the curve in the s_{++} case. In d-wave superconductors ξ_h/ξ_{c2} always increases with Γ. For $d_{x^2-y^2}$ pairing the nonlocal generalized London equation and its connection with the Eilenberger theory are also considered. The problem of the effective penetration depth in the vortex state for d-wave superconductors is discussed. In this case, the field dependence of λ_{eff} is connected with the extended quasiclassical state near the nodes of the superconducting gap.

Author details

I. Zakharchuk, P. Belova, K. B. Traito and E. Lähderanta
Lappeenranta University of Technology, Finland

6. References

[1] Q. Li, Y. N. Tsay, M. Suenaga, R. A. Klemm, G. D. Gu, and N. Koshizuka. *Phys. Rev. Lett.*, 83:4160, 1999.
[2] R. A. Klemm. *Int. J. Mod. Phys. B*, 12:2920, 1983.
[3] D. R. Harshman, W. J. Kossler, X. Wan, A. T. Fiory, A. J. Greer, D. R. Noakes, C. E. Stronach, E. Koster, and J. D. Dow. *Phys. Rev. B*, 69:174505, 2004.
[4] A. G. Sun, D. A. Cajewski, M. B. Maple, and R. C. Dynes. *Phys. Rev. Lett.*, 72:2267, 1994.
[5] D. A. Wollmann, D. J. Van Harlingen, J. Giapintzakis, and D. M. Ginsberg. *Phys. Rev. Lett.*, 74:797, 1995.
[6] J. P. Rice, N. Rigakis, D. M. Ginsberg, and J. M. Mochel. *Phys. Rev. B*, 46:11050, 1992.
[7] C. C. Tsuei, J. R. Kirtley, C. C. Chi, L. S. Yu-Jahnes, A. Gupta, T. Shaw, J. Z. Sun, and M. B. Ketchen. *Phys. Rev. Lett.*, 73:593, 1994.
[8] Y. Kamihara, T. Watanabe, M. Hirano, and H. Hosono. *J. Am. Chem. Soc.*, 130:3296, 2008.

[9] X.C. Wang, Q.Q. Liu, Y.X. Lv, W.B. Gao, L.X. Yang, R.C. Yu, F.Y. Li, and C.Q. Jin. *Solid State Commun.*, 148:538, 2008.
[10] I. I. Mazin, D. J. Singh, M. D. Johannes, and M. H. Du. *Phys. Rev. Lett.*, 101:057003, 2008.
[11] K. Kuroki, S. Onari, R. Arita, H. Usui, Y. Tanaka, H. Kontani, and H. Aoki. *Phys. Rev. Lett.*, 101:087004, 2008.
[12] K. Seo, B. A. Bernevig, and J. Hu. *Phys. Rev. Lett.*, 101:206404, 2008.
[13] H. Kontani and S. Onari. *Phys. Rev. Lett.*, 104:157001, 2010.
[14] Y. Yanagi, Y. Yamakawa, and Y. Ōno. *Phys. Rev. B*, 81:054518, 2010.
[15] H. Ding, K. Nakayama P. Richard and, K. Sugawara, T. Arakane, Y. Sekiba, A. Takayama, S. Souma, T. Sato, T. Takahashi, Z. Wang, X. Dai, Z. Fang, G. F. Chen, J. L. Luo, and N. L. Wang. *Europhys. Lett.*, 83:47001, 2008.
[16] L. Wray, D. Qian, D. Hsieh, Y. Xia, L. Li, J. G. Checkelsky, A. Pasupathy, K.K. Gomes, C.V. Parker, A.V. Fedorov, G. F. Chen, J. L. Luo, A. Yazdani, N. P. Ong, N. L. Wang, and M. Z. Hasan. *Phys. Rev. B*, 78:184508, 2008.
[17] Z. H. Liu, P. Richard, K. Nakayama, G.-F. Chen, S. Dong, J. B. He, D. M. Wang, T.-L. Xia, K. Umezawa, T. Kawahara, S. Souma, T. Sato, T. Takahashi, T. Qian, Y. Huang, N. Xu, Y. Shi, H. Ding, and S. C. Wang. *Phys. Rev. B*, 84:064519, 2011.
[18] A. D. Christianson, E. A. Goremychkin, R. Osborn, S. Rosenkranz, M. D. Lumsden, C. D. Malliakas, I. S. Todorov, H. Claus, D. Y. Chung, M. G. Kanatzidis, R. I. Bewley, and T. Guidi. *Nature (London)*, 456:930, 2008.
[19] T. Hanaguri, S. Niitaka, K. Kuroki, and H. Takagi. *Science*, 328:474, 2010.
[20] S. Onari, H. Kontani, and M. Sato. *Phys. Rev. B*, 81:060504(R), 2010.
[21] S. Onari and H. Kontani. *Phys. Rev. Lett.*, 103:177001, 2009.
[22] C. Tarantini, M. Putti, A. Gurevich, Y. Shen, R. K. Singh, J. M. Rowell, N. Newman, D. C. Larbalestier, P. Cheng, Y.Jia, and H.-H. Wen. *Phys. Rev. Lett.*, 104:087002, 2010.
[23] G. R. Stewart. *Rep. Prog. Phys.*, 83:1589, 2011.
[24] P. J. Hirschfeld and N. Goldenfeld. *Phys. Rev. B*, 48:4219, 1993.
[25] K. Hashimoto, T. Shibauchi, S. Kasahara, K. Ikada, S. Tonegawa, T. Kato, R. Okazaki, C. J. van der Beek, M. Konczykowski, H. Takeya, K. Hirata, T. Terashima, and Y. Matsuda. *Phys. Rev. Lett.*, 102:207001, 2009.
[26] L. Luan, T. M. Lippman, C. W. Hicks, J. A. Bert, O. M. Auslaender, J.-H. Chu, J. G. Analytis, I. R. Fisher, and K. A. Moler. *Phys. Rev. Lett.*, 106:067001, 2011.
[27] M. A. Tanatar, J.-Ph. Reid, H. Shakeripour, X. G. Luo, N. Doiron-Leyraud, N. Ni, S. L. Bud'ko, P. C. Canfield, R. Prozorov, and L. Taillefer. *Phys. Rev. Lett.*, 104:067002, 2010.
[28] J. D. Fletcher, A. Serafin, L. Malone, J. G. Analytis, J.-H. Chu, A. S. Erickson, I. R. Fisher, and A. Carrington. *Phys. Rev. Lett.*, 102:147001, 2009.
[29] C. W. Hicks, T. M. Lippman, M. E. Huber, J. G. Analytis, J.-H. Chu, A. S. Erickson, I. R. Fisher, and K. A. Moler. *Phys. Rev. Lett.*, 103:127003, 2009.
[30] K. Hashimoto, M. Yamashita, S. Kasahara, Y. Senshu, N. Nakata, S. Tonegawa, K. Ikada, A. Serafin, A. Carrington, T. Terashima, H. Ikeda, T. Shibauchi, and Y. Matsuda. *Phys. Rev. B*, 81:220501(R), 2010.
[31] Y. Nakai, T. Iye, S. Kitagawa, K. Ishida, S. Kasahara, T. Shibauchi, Y. Matsuda, and T. Terashima. *Phys. Rev. B*, 81:020503(R), 2010.
[32] M. Yamashita, Y. Senshu, T. Shibauchi, S. Kasahara, K. Hashimoto, D. Watanabe, H. Ikeda, T. Terashima, I. Vekhter, A. B. Vorontsov, and Y. Matsuda. *Phys. Rev. B*, 84:060507(R), 2011.

[33] J. K. Dong, S. Y. Zhou, T. Y. Guan, H. Zhang, Y. F. Dai, X. Qiu, X. F. Wang, Y. He, X. H. Chen, and S. Y. Li. *Phys. Rev. Lett.*, 104:087005, 2010.
[34] K. Hashimoto, A. Serafin, S. Tonegawa, R. Katsumata, R. Okazaki, T. Saito, H. Fukazawa, Y. Kohori, K. Kihou, C. H. Lee, A. Iyo, H. Eisaki, H. Ikeda, Y. Matsuda, A. Carrington, and T. Shibauchi. *Phys. Rev. B*, 82:014526, 2010.
[35] G. Xu, H. Zhang, X. Dai, and Z. Fang. *Europhys. Lett.*, 84:67015, 2008.
[36] R. Thomale, C. Platt, W. Hanke, and B. A. Bernevig. *Phys. Rev. Lett.*, 106:187003, 2011.
[37] Y. J. Yan, X. F. Wang, R. H. Liu, H. Chen, Y. L. Xie, J. J. Ying, and X. H. Chen. *Phys. Rev. B*, 81:235107, 2010.
[38] N. Ni, S. L. Bud'ko, A. Kreyssig, S. Nandi, G. E. Rustan, A. I. Goldman, S. Gupta, J. D. Corbett, A. Kracher, and P. C. Canfield. *Phys. Rev. B*, 78:014507, 2008.
[39] C. Martin, R. T. Gordon, M. A. Tanatar, H. Kim, N. Ni, S. L. Bud'ko, P. C. Canfield, H. Luo, H. H. Wen, Z. Wang, A. B. Vorontsov, V. G. Kogan, and R. Prozorov. *Phys. Rev. B*, 80:020501(R), 2009.
[40] M. Rotter, M. Tegel, and D. Johrendt. *Phys. Rev. Lett.*, 101:107006, 2008.
[41] Y. Zhang, L. X. Yang, F. Chen, B. Zhou, X. F. Wang, X. H. Chen, M. Arita, K. Shimada, H. Namatame, M. Taniguchi, J. P. Hu, B. P. Xie, and D. L. Feng. *Phys. Rev. Lett.*, 105:117003, 2010.
[42] S.W. Zhang, L. Ma, Y. D. Hou, J. Zhang, T.-L. Xia, G. F. Chen, J. P. Hu, G. M. Luke, and W. Yu. *Phys. Rev. B*, 81:012503, 2010.
[43] T. Sato, K. Nakayama, Y. Sekiba, P. Richard, Y.-M. Xu, S. Souma, T. Takahashi, G. F. Chen, J. L. Luo, N. L. Wang, and H. Ding. *Phys. Rev. Lett.*, 103:047002, 2009.
[44] R. Thomale, C. Platt, W. Hanke, J. Hu, and B. A. Bernevig. *Phys. Rev. Lett.*, 107:117001, 2011.
[45] J. H. Tapp, Z. J. Tang, B. Lv, K. Sasmal, B. Lorenz, P. C. W. Chu, and A. M. Guloy. *Phys. Rev. B*, 78:060505(R), 2008.
[46] D. J. Singh. *Phys. Rev. B*, 78:094511, 2008.
[47] I. A. Nekrasov, Z.V. Pchelkina, and M.V. Sadovskii. *JETP Lett.*, 88:543, 2008.
[48] R. A. Jishi and H. M. Alyahyaei. *Adv. Condens. Matter Phys.*, 2010:1, 2010.
[49] S. J. Zhang, X. C. Wang, R. Sammynaiken, J. S. Tse, L. X. Yang, Z. Li, Q. Q. Liu, S. Desgreniers, Y. Yao, H. Z. Liu, and C. Q. Jin. *Phys. Rev. B*, 80:014506, 2009.
[50] F. L. Pratt, P. J. Baker, S. J. Blundell, T. Lancaster, H. J. Lewtas, P. Adamson, M. J. Pitcher, D. R. Parker, and S. J. Clarke. *Phys. Rev. B*, 79:052508, 2009.
[51] C.W. Chu, F. Chen, M. Gooch, A.M. Guloy, B. Lorenz, B. Lv, K. Sasmal, Z.J. Tang, J.H. Tapp, and Y.Y. Xue. *Physica C*, 469:326, 2009.
[52] S. V. Borisenko, V. B. Zabolotnyy, D. V. Evtushinsky, T. K. Kim, I. V. Morozov, A. N. Yaresko, A. A. Kordyuk, G. Behr, A. Vasiliev, R. Follath, and B. Büchner. *Phys. Rev. Lett.*, 105:067002, 2010.
[53] K. Umezawa, Y. Li, H. Miao, K. Nakayama, Z.-H. Liu, P. Richard, T. Sato, J. B. He, D.-M. Wang, G. F. Chen, H. Ding, T. Takahashi, and S.-C. Wang. *Phys. Rev. Lett.*, 108:037002, 2012.
[54] R. Laiho, M. Safonchik, and K. B. Traito. *Phys. Rev. B*, 76:140501(R), 2007.
[55] R. Laiho, M. Safonchik, and K. B. Traito. *Phys. Rev. B*, 78:064521, 2008.
[56] J. E. Sonier. *Rep. Prog. Phys.*, 70:1717, 2007.
[57] P. deGennes. *Superconductivity of Metals and Alloys*, pages Addison–Wesley, New York, 1989.

[58] V. G. Kogan, A. Gurevich, J. H. Cho, D. C. Johnston, M. Xu, J. R. Thompson, and A. Martynovich. *Phys. Rev. B*, 54:12386, 1996.
[59] E. H. Brandt. *Phys. Rev. B*, 37:2349(R), 1988.
[60] E. H. Brandt. *Physica C*, 195:1, 1992.
[61] I. G. de Oliveira and A. M. Thompson. *Phys. Rev. B*, 57:7477, 1998.
[62] J. R. Clem. *J. Low Temp. Phys*, 18:427, 1975.
[63] Z. Hao, J. R. Clem, M. W. McElfresh, L. Civale, A. P. Malozemoff, and F. Holtzberg. *Phys. Rev. B*, 43:2844, 1991.
[64] A. Yaouanc, P. Dalmas de Reotier, and E. H. Brandt. *Phys. Rev. B*, 55:11107, 1997.
[65] W. V. Pogosov, K. I. Kugel, A. L. Rakhmanov, and E. H. Brandt. *Phys. Rev. B*, 64:064517, 2001.
[66] A. Maisuradze, R. Khasanov, A. Shengelaya, and H. Keller. *J. Phys.: Condens. Matter*, 21:S075701, 2009.
[67] L. Kramer and W. Pesch. *Z. Phys.*, 269:59, 1974.
[68] M. Ichioka, A. Hasegawa, and K. Machida. *Phys. Rev. B*, 59:8902, 1999.
[69] M. Ichioka, A. Hasegawa, and K. Machida. *Phys. Rev. B*, 59:184, 1999.
[70] M. H. S. Amin, I. Affleck, and M. Franz. *Phys. Rev. B*, 58:5848, 1998.
[71] I. Affleck, M. Franz, and M. H. Sharifzadeh Amin. *Phys. Rev. B*, 55, 1997.
[72] M. Franz, I. Affleck, and M. H. S. Amin. *Phys. Rev. Lett.*, 79:1555, 1997.
[73] M. H. S. Amin, M. Franz, and I. Affleck. *Phys. Rev. Lett.*, 84:5864, 2000.
[74] A. B. Vorontsov, M. G. Vavilov, and A. V. Chubukov. *Phys. Rev. B*, 79:140507(R), 2009.
[75] W. A. Huttema, J. S. Bobowski, P. J. Turner, R.Liang, W. N. Hardy, D. A. Bonn, and D. M. Broun. *Phys. Rev. B*, 80:104509, 2009.
[76] V. G. Fleisher, Yu. P. Stepanov, K. B. Traito, E. Lähderanta, and R. Laiho. *Physica C*, 264:295, 1996.
[77] P. Miranović, M. Ichioka, and K. Machida. *Phys. Rev. B*, 70:104510, 2004.
[78] Y. N. Ovchinnikov and V. Z. Kresin. *Phys. Rev. B*, 52:3075, 1995.
[79] J. E. Sonier. *J. Phys.: Condens. Matter*, 16:S4499, 2004.
[80] J. E. Sonier, W. Huang, C. V. Kaiser, C. Cochrane, V. Pacradouni, S. A. Sabok-Sayr, M. D. Lumsden, B. C. Sales, M. A. McGuire, A. S. Sefat, and D. Mandrus. *Phys. Rev. Lett.*, 106:127002, 2011.
[81] D. S. Inosov, J. S. White, D. V. Evtushinsky, I. V. Morozov, A. Cameron, U. Stockert, V. B. Zabolotnyy, T. K. Kim, A. A. Kordyuk, S. V. Borisenko, E. M. Forgan, R. Klingeler, J. T. Park, S. Wurmehl, A. N. Vasiliev, G. Behr, C. D. Dewhurst, and V. Hinkov. *Phys. Rev. Lett.*, 104:187001, 2010.
[82] G. Yin and K. Maki. *Physica B*, 194-196:2025, 1994.
[83] A. B. Pippard. *Proc. R. Soc. London A*, 216:547, 1953.
[84] V. G. Kogan, M. Bullock, B. Harmon, P. Miranovic̀, Lj. Dobrosavljevic̀-Grujic̀, P. L. Gammel, and D. J. Bishop. *Phys. Rev. B*, 55:8693 (R), 1997.
[85] D. Xu, S. K. Yip, and J. A. Sauls. *Phys. Rev. B*, 51:16233, 1995.
[86] I. Kosztin and A. J. Leggett. *Phys. Rev. Lett.*, 79:135, 1997.
[87] D. Rainer, J. A. Sauls, and D. Waxman. *Phys. Rev. B*, 54:10094, 1996.
[88] F. Gygi and M. Schluter. *Phys. Rev. B*, 41:822, 1990.
[89] T. Dahm, S. Graser, C. Iniotakis, and N. Schopohl. *Phys. Rev. B*, 66:144515, 2002.
[90] M. Franz and Z. Teŝanovic̀. *Phys. Rev. Lett.*, 80:4763, 1998.
[91] M. Kato and K. Maki. *Physica B*, 284:739, 2000.
[92] A. Zare, A. Markowsky, T. Dahm, and N. Schopohl. *Phys. Rev. B*, 78:104524, 2008.

[93] P. Belova, K. B. Traito, and E. Lähderanta. *J. Appl. Phys.*, 110:033911, 2011.
[94] N. Nakai, P. Miranovic, M. Ichioka, H. F. Hess, K. Uchiyama, H. Nishimori, S. Kaneko, N. Nishida, and K. Machida. *Phys. Rev. Lett.*, 97:147001, 2006.
[95] L. Kramer and W. Pesch. *J. Low Temp. Phys.*, 15:367, 1974.
[96] R. Laiho, E. Lähderanta, M. Safonchik, and K. B. Traito. *Phys. Rev. B*, 71:024521, 2005.
[97] Y. Ren, J.-H. Xu, and C. S. Ting. *Phys. Rev. Lett.*, 74:3680, 1995.
[98] R. Laiho, M. Safonchik, and K. B. Traito. *Phys. Rev. B*, 73:024507, 2006.
[99] D. C. Johnston. *Advances in Physics*, 59:803, 2010.